Dalton Transactions

Accepted Manuscript

ROYAL SOCIETY OF CHEMISTRY

www.rsc.org/dalton

FOR TABLE OF CONTENTS

The synthesis route followed to prepare h-WO_3 type oxides results in the production of nanostructured crystals by spontaneous formation of self-assembled and regular nano-cavities in its surface.

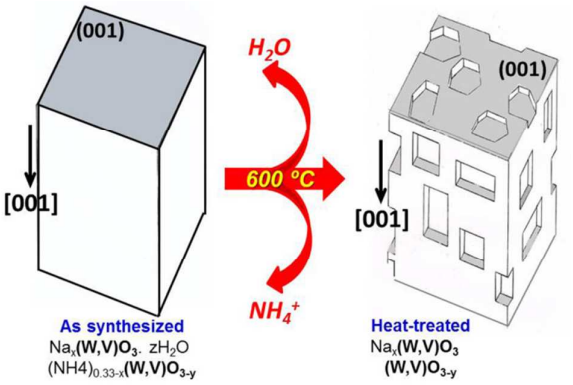

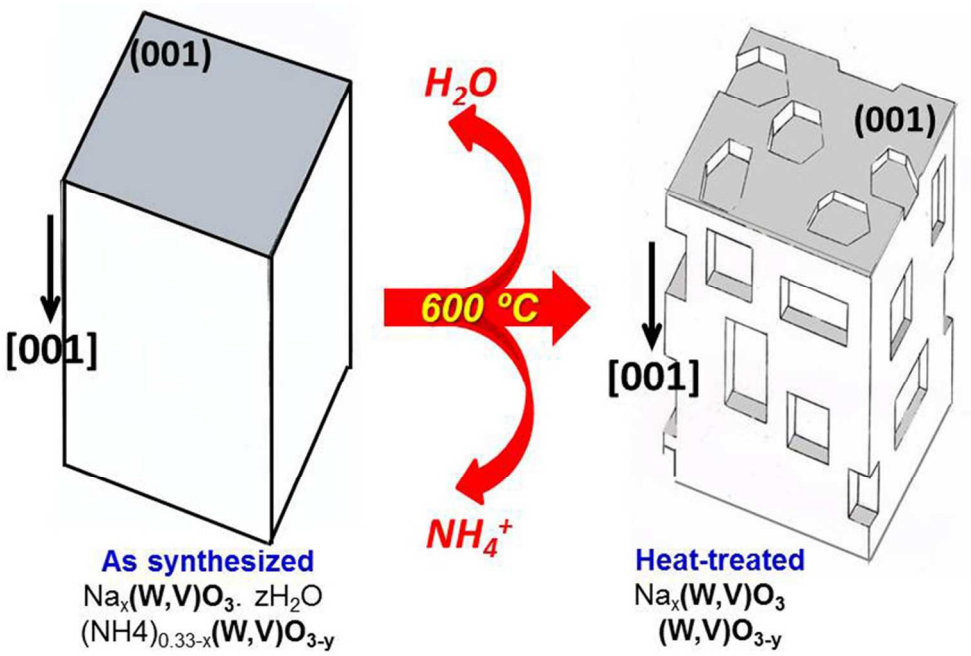

Figure for Table of Contents
82x54mm (300 x 300 DPI)

On the Origin of the Spontaneous Formation of Nanocavities in Hexagonal Bronzes (W, V)O_3

E. García-González[1*], M. D. Soriano[2], E. Urones-Garrote [3] and J.M. López Nieto[2]

[1] Departamento Química Inorgánica, Facultad de Ciencias Químicas, Universidad Complutense, 28040 Madrid, Spain.

[2] Instituto de Tecnología Química, UPV-CSIC, Campus Universidad Politécnica de Valencia, Avenida de los Naranjos s/n, 46022 Valencia, Spain.

[3] Centro Nacional de Microscopia Electrónica, Universidad Complutense, E-28040, Madrid, Spain.

KEYWORDS: nanocavities, h-(WO_3), tungsten bronzes, HAADF-STEM

FOR TABLE OF CONTENTS ENTRY

The synthesis route followed to prepare h-WO_3 type oxides results in the production of nanostructured crystals by spontaneous formation of self-assembled and regular nano-cavities in its surface.

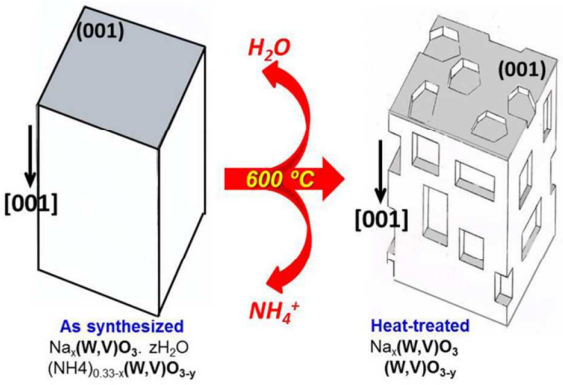

ABSTRACT

Hexagonal $(W,V)O_{3-x}$ oxides of high thermal stability have been synthesized hydrothermally through the intermediate products $Na_x(W,V)O_3.zH_2O$ and $(NH_4)_{0.33-x}(W,V)O_{3-y}$. The obtained crystals show nanostructured surface via the formation of a dense population of polyhedral nanocavities self-distributed along particular crystallographic directions. Nanocavities present a regular size that ranges from 5 to 10 nm in both length and width. The synthesis process involves highly topotactic relationship between the as synthesized product and the desired final product and this fact is proposed as the origin of the surface nanostructure. Comparison of our results with observations in different solids has allowed us to suggest that formation of nanocavities is an extensive spontaneous process when materials are obtained by chemical reactions of solids leading to products with defined crystallographic orientation with respect to the original compound. The characterization performed provides evidence about the potential relevance nanocavities would have in the functional properties of the resulting solids.

INTRODUCTION

Tungsten oxides are materials of huge interest due to their many known applications in electrochromic devices,[1] gas sensors[2] and photocatalysts.[3] WO_3 exhibits different structural modifications and among them hexagonal *h*-WO_3 (the so called HTB structure) is of considerable interest due to its open structure to be used as a selective host for intercalation and exchange chemistry.[4] As in other transition metal oxides, the suitable combination of W with different cations can be exploited to enhance WO_3 properties or even to extend them. In this sense, the partial substitution of W by Mo in *h*-WO_3 has been recently reported as a way to improve its NH_3-sensing properties.[5] Additionally, this substitution provides modification in the ion exchange selectivity of the material.[4c] *h*-WO_3 is also known as an effective catalyst in several acid catalyzed reactions.[6] The addition of vanadium to the structural framework of *h*-WO_3 transforms the material into a bifunctional catalyst with acidic and redox properties simultaneously. These materials were recently tested as efficient in the selective transformation of glycerol to acrylic acid.[7]

Moreover, crystal morphology as well as structure stability can be controlled through adequate additives in the process of synthesis. In this sense, template-free strategies have been used to prepare nanoporous polycrystalline particles of different metal oxides from oxalates. [8] Recent investigations have been done in the hydrothermal production of nanostructured alkali tungstates M_xWO_3 that demonstrate how the morphology of the HTBs can be tuned by the choice of appropriate reactives.[9] In the same way, the shape of nanoscale hexagonal W/Mo-oxides can be expanded into a variety of morphologies in a controlled way via the use of different alkali chlorides as hydrothermal additives. [10] There is a complex relationship between the internal W/Mo substitution in the hexagonal structure and the external morphological influence of the additive cation

allocated in the hexagonal tunnels. [10,11] The influence of composition on nanosized *h*-WO_3 prepared from annealing of $(NH_4)_{0.33-x}WO_{3-y}$ on applications such as conductivity and gas sensitivity, has been investigated and the study also revealed [4a] a correlation between the amount and nature of residual ions in the hexagonal tunnels and the stability of *h*-WO_3.

Besides to controlled composition, transformation of these tungsten-based materials into nanostructured materials is of high relevance. Various nanostructures of WO_3, such as nanorods, [12] nanoplates [13] or nanodiscs, [14] have been successfully fabricated by a variety of methods. Hierarchical structures assembled from the above nanostructures have been also obtained that present outstanding electrochemical properties [15] or important advantages in their adsorption performance due to their high surface area**.**[16] Hence, micro/nanostructural and/or topological aspects may also play a crucial role in the behavior of these W-based metal oxide bronzes.

In this sense, we present in this paper the transformation of both $Na_x(W,V)O_3.zH_2O$ and $(NH_4)_{0.33-x}(W,V)O_{3-y}$ into nanostructured *h*-$(W,V)O_{3-x}$. Crystals surface show the formation of a dense population of polyhedral nanocavities self-distributed along particular crystallographic directions. Nanocavities are isolated nanoscale structures inside a solid, open to the surface and that do not connect together like nanopores. However, they are relevant constituents in the development of different properties and this is the case of some photo-electrochemical systems. [17, 18] Empty space has been also presented as a relevant part of any nanostructured system where chemistry occurs,[19] offering extra access to important active sites. In any chemical system the spacial arrangement of significant chemical/topological sites is a crucial point for all potential applications in which a well-defined and easily accessible crystal surface is required. In

this scenario and provided the potential significance of our finding, we present here the results obtained in the investigation of this nanostructure.

EXPERIMENTAL SECTION

Samples preparation

Vanadium free and vanadium-containing h-WO_3 samples were prepared by hydrothermal synthesis from aqueous solution of three different precursors: i) $Na_2WO_4{\cdot}2H_2O$; ii) $(NH_4)_6H_2W_{12}O_{40}{\cdot}H_2O$; and iii) a mixture of $(NH_4)_6H_2W_{12}O_{40}{\cdot}H_2O$ and NaCl. For V-free samples oxalic acid was used as a reductor (with an oxalic acid/W molar ratio of 0.07). V-containing samples were prepared by adding vanadyl sulphate (with a V/W atomic ratio of 0.20). In all cases, gels were loaded in Teflon-lined stainless-steel autoclaves and heated at 175ºC for 48h. The obtained solids were filtered off, washed and dried at 100ºC for 16 h. In order to obtain the final crystal phase, the solids were heat-treated at 450º C (V-free materials) or 600º C (V- containing materials) during 2 hours in a N_2 stream. The synthesis parameters are shown in Table 1.

Corresponding samples were named as (Na)**W-O**, (NH_4)**W-O**, (Na/NH_4)**W-O** and (Na)**W/V-O**, (NH_4)**W/V-O,** (Na/NH_4)**W/V-O** for the V-free and V-containing series, respectively.

Samples characterization

Powder X-ray diffraction patterns (XRD) were collected by using an Enraf Nonius FR590 sealed tube diffractometer, with monochromatic $CuK_{\alpha 1}$ radiation operating at 40 kV and 30 mA.

Thermogravimetric measurements were carried out on a Mettler-Toledo TGA/SDTA 851 instrument in the temperature range 20–600 ºC with 0.02 g samples (heating rate 10

ºC min^{-1} and air flow 100 ml min^{-1}). For the DTA / MS curves the measurements were performed in the 20–500 ºC temperature range (heating rate 10 ºC min^{-1}, 5% O_2/He, flow 25 ml min^{-1})**.** The relative masses corresponding to the main degradation compounds were analyzed with a mass spectrometer (Thermostar Balzers) coupled with the apparatus.

Samples for transmission electron microscopy (TEM) were ultrasonically dispersed in n-butanol and transferred to carbon coated copper grids. Selected area electron diffraction (SAED) and high resolution transmission electron microscopy (HRTEM) were carried out on a JEOL JEM3000F electron microscope (point resolution of 0.17 nm). In order to determine the W/V cationic ratio, crystal by crystal XEDS microanalysis was performed by using the same microscope equipped with an X-ray microanalysis ISIS 300 (Oxford Instruments) with a detector model LINK "Pentafet" (resolution 135 eV).

The microscope is equipped with a Scanning-TEM (STEM) unit and a high-angle annular dark-field (HAADF) detector. Z-contrast images were acquired using a collection angle of ~ 60 mrad. Electron energy-loss spectroscopy (EELS) data sets were acquired in STEM mode as line-scans with an ENFINA 1000 spectrometer (electron probe diameter of ~ 0.3 nm). The acquired low-loss spectra included the zero-loss peak and the plasmon peaks, so that sample thickness can be computed from each spectra.[20]

BET specific surface areas were measured on a Micromeritics TriStar 3000 instrument, with adsorption of N_2 at -76 ºC. Catalytic tests for the partial oxidation of H_2S to sulfur were carried out in a fixed-bed quartz tubular flow reactor, in the 180–260 ºC temperature range at atmospheric pressure. A total flow (130 mL min^{-1}) with H_2S/air/He molar ratio of 1.2/5.0/93.8 and a catalyst weight of 0.1 g were used. Analysis of

reactants and reaction products was carried out online by using gas chromatography and two different chromatographic columns (Molecular Sieve 5A and Porapak T).[21]

RESULTS AND DISCUSSION

The powder X-ray diffraction data of the as prepared samples did not show significant differences from the undoped samples to the vanadium-containing samples (figures S1 and S2 in Supplementary Information). They could be assigned directly to the hexagonal phase $Na_xWO_{3+x/2}.zH_2O$, [22] very close to h-WO_3 (ICDD 33-1387) or to the hexagonal ammonium tungsten bronze $(NH_4)_{0.33-x}WO_{3-y}$ (ICDD 42-0452), depending on the precursor used in the synthesis procedure. For heat-treated samples leading to the HTB-type phase (Table 2), all the diffraction patterns were equally interpreted and the diffraction maxima could be indexed according to the unit cell of *h*-WO_3 (ICDD 33-1387, space group P*6/mmm*, cell parameters *a*= 0.7298 nm, *c*= 0.3899 nm).

Our initial interest concerning the preparation of hexagonal bronzes with empty tunnels, led us to use ammonium tungstate as precursor and the hydrothermal process gave rise to the orthorhombic $WO_3.1/3H_2O$ as synthesis product. Further calcination, however, stabilized only the monoclinic m-WO_3 phase. As we previously stated, [7] and in contrast with the process described in the literature, [23-25] the stabilization of the *h*-WO_3 phase requires the addition of a reducer such as oxalic acid using either Na^+, NH_4^+ or the mixture of both as template. In addition, the thermal stability is limited and it turns into m-WO_3 at temperatures above 450º C (figure S1 and Table 2).

For the synthesis of the vanadium-containing samples no addition of oxalic acid was required and a hexagonal type phase was also directly obtained from the hydrothermal

process. Heat-treatment of these samples did show an increase of the thermal stability of *h*-$(W,V)O_3$ up to 600º C (Table 2 and Figure S2).

The structural/microstructural aspects of the heat-treated samples were further studied in detail by Transmission Electron Microscopy. Results were in agreement with what we observed from powder X-ray diffraction data and heat-treated samples were constituted by *h*-WO_3 as single phase. For V-containing samples, XEDS was used to determine the W/V cationic ratio on each crystal. The microanalysis performed showed that vanadium was homogeneously incorporated in all the crystals, being $W_{0.9}V_{0.1}O_{3-x}$ the average composition.

Crystals grew always in a preferential mode along the [001] direction giving rise to a characteristic rod like morphology with typical length and width values of 0.5-2 μm and 0.1-0.3 μm, respectively. Only vanadium doped samples prepared from sodium tungstate as precursor, showed plate-like crystal growth in the (001) plane, the crystals showing an average size between 1.5-2 μm. Samples prepared with the mixture of sodium and ammonium tungstate contained both type of crystals. It seems, therefore, that under the synthesis conditions employed here, Na^+ cations act as templates for preferential growth in the *ab* plane.

Figure 1 shows the selected area electron diffraction (SAED) patterns corresponding to three different crystals of $(W,V)O_3$ heat treated at 600º C in the (a) [100], (b) $[1\bar{1}0]$ and (c) [001] zone axes. Although no evidence for doubling of the *c* axis was apparent in the X-ray diffraction patterns, (0 0 *l/2*) reciprocal lattice points are clearly observed (see figures 1(a) and 1(b)). According to this fact, diffraction maxima in the three projections are indexed on the basis of the hexagonal cell P*6₃/mcm,* a= 0.73 nm, c= 0.78 nm. [26]

Octahedra tilting in the HTB-type compounds always seems to be observed and it has been previously reported as related to the doubled periodicity along *c*. [27, 28]

At this point it is important to mention that all the samples preserving the hexagonal type phase after the final thermal treatment show very similar electron diffraction patterns, independently of the cation used as template.

Despite the hexagonal form is the only crystal phase observed by X-ray diffraction, electron diffraction patterns from our samples show always sharp elongation of diffraction maxima along [010] ([100]), [110] and equivalent reciprocal directions and diffraction patterns shown in figure 1 illustrate very well this fact. This is indicative of certain degree of disorder along these directions. It appears both in crystals of samples prepared with sodium or with ammonium cations. In addition, the electron diffraction pattern of some crystals in the $[1\bar{1}0]$ projection presents a weak diffraction maximum doubling [111] and equivalent directions. It does not belong to the hexagonal phase as described but it can be assigned to the (101) maximum of the monoclinic phase m-WO_3 [29] to which the hexagonal form evolves when increasing temperature. [30,31] The transformation *h*-$WO_3 \rightarrow$ *m*-WO_3 occurs in a topotactic way as previously proposed by Figlarz [30] and the monoclinic phase begins to grow from the (100) planes in the $(200)_h$ planes, provided their similarity. The schematic representation of Figure S3(a) illustrates the intergrowth of both polymorphs in two different projections. This information provides a reliable interpretation for the streaking of the diffraction maxima observed as well as for the weak extra diffraction maximum doubling [111]. The transformation of h-WO_3 to the stable monoclinic polymorph is reported to occur slightly above 400º C. [30] In our case and for the V-containing samples, transition begins at 600º C, as demonstrated by the electron diffraction study. At the early stages of the

transformation streaking of diffraction maxima occur as a consequence of disorder in a short range. As it goes on, regions of the new phase become apparent, as shown in Figure S3(b) on a crystal of h-$(W,V)O_3$ heat treated at 600 ºC and oriented in the $[100]_h$ projection.

Figure 2 shows the high resolution electron micrographs of three different crystals of $(W,V)O_3$ heat treated at 600º C in the (a) [100], (b)) $[1\bar{1}0]$ and (c) [001] projections. The image contrasts can be easily identified and correspond to the main directions of the HTB-type unit cell. In addition, areas with double periodicity along [001] can be distinguished (see figure 2b).

A remarkable property of these heat-treated materials concerns the crystals surface. A well disperse and dense distribution of polyhedral nanocavities is always observed in all the samples independently of the growth mode. From the careful observation of the images contrast on figure 2, the presence of the polyhedral cavities can be deduced, although they are better observed in slightly tilted orientation and in out of focus conditions. They appear as hollow (their nature will be further probed and explained) and well oriented polyhedra with faces parallel to [010] and [001] in the [100] projection (figure 2a), to [110] and [001] in the $[1\bar{1}0]$ projection (figure 2b) or parallel to $[1\bar{2}0]$ or [210] in the [001] projection (figure 2c).

Nanocavities present a regular size that ranges from 5 to 10 nm in both length and width. Pristine samples do not show cavities or irregular features in their surfaces. These nanovoids can be observed in the surface of the crystals after heat-treatments at temperature of ~200 ºC. At this low temperature the surface of the crystals exhibit a porous sponge–like aspect (figure 3(a)) and the irregular pores turn into regular voids

self-assembled along certain directions when increasing temperature up to 600 ºC (figure 3(b)).

We have further investigated the as synthesized materials by thermal analysis. Samples pass through different thermal transformations in the temperature range RT-600º C as shown by the corresponding thermogravimetric analysis (figure 4). The structure of the hydrous oxide $Na_xWO_{3+x/2}.zH_2O$ is very close to that of the high temperature HTB except by the fact that it contains Na^+ ions in the hexagonal windows together with disordered water molecules in the hexagonal tunnels.[22] In the same way, NH_4^+ ions are placed in the hexagonal tunnels of the ammonium tungsten bronze $(NH_4)_{0.33-x}WO_{3-y}$.

The low temperature (25 - 600º C) thermal transformations of $Na_xWO_{3+x/2}.zH_2O$ have been recently investigated by means of TG/DTA, ^{23}Na NMR and X-ray and neutron diffraction. [4c, 32] From their detailed study, authors demonstrate that water evolution occurs stepwise as a consequence of the Na-rearrangement which takes place through the formation of different Na-species. Heating at 100 ºC mainly produces tunnel dehydration but at 200 ºC the first structural transformation occurs and Na is distributed between the planar hexagonal positions and a new position which is in the center of the cavity between two hexagonal windows. Authors claimed that sodium rearrangement in the tunnels forces the residual water content into pocketed and regionalized occlusions and it is not distributed throughout the tunnels. After heating at 300º C, the entire system undergoes the transformation, with all the Na inside the tunnels. The overall process is accompanied by a progressive decrease in the volume of the unit cell.

In the case of the hexagonal ammonium tungsten bronze $(NH_4)_{0.33-x}WO_{3-y}$ it has been reported that ammonium leave the structure in three overlapping steps between 250 and 500º C, [4a] the first being those ions bonded the weakest and closer to the surface which

evolve together with water up to 200-250º C. Around this temperature and up to 500ºC, NH_4^+ ions located in the hexagonal tunnels of the structure are eliminated.

All the above features find a strong parallelism in the thermal decomposition of our samples. The thermogravimetric analysis of the Na-containing samples is shown in figure 4a. There is a broad endothermic peak at about 230 – 250º C on each thermogram which corresponds to a net weight loss of ~ 2.5–2.7%. This is in agreement with the previous observations [4c, 32] and with the fact that it is about 250º C when the first structural transformation occurs. The vanadium free sample shows in addition an endothermic peak at ~ 80-90º C which can be assigned to the first water evolution. This is not observed in the V-containing sample where the plate like morphology associated to preferential growth on the *ab* plane makes the length of the tunnels significantly shorter.

The thermogravimetric analysis of the NH_4^+-containing samples is shown in figure 4b. In addition to the endothermic peak at 80-90º C assigned to the first water evolution, two other broad endothermic peaks partially overlapped are observed between 200 and 500º C in agreement with previous data. [4a] The thermal analysis of Na^+/NH_4^+-containing samples (figure 4c) presents strong similarity with those containing only NH_4^+. The same features as above are observable and the weight loss takes place within the same temperature interval.

Therefore, it is a common fact that the first step in the weight loss takes place at a temperature about 200º C, and it is around this temperature when tunnels start to empty and former structures begin to transform into the final hexagonal bronze. It is precisely above this temperature when nanocavities appear on the surface of the crystals. This is

consistent with the fact that pristine samples do not show cavities or irregular features in their surfaces.

The creation of dense regular polyhedral nanocavities reported for TiO_2 by adequately choosing the synthesis precursor, has been explained by using the "anti-crystal growth" model. [18] The suitable hydrothermal route produces $H_2Ti_3O_7$, whose dehydration gives rise to B-TiO_2 [33] or TiO_2-anatase [18] with dense nanocavities. There is certain degree of topotaxy between $H_2Ti_3O_7$ and TiO_2-anatase and *d* spacing of (001) and (010) planes are very similar in both structures. However, the unit cell of TiO_2 is much denser and the evaporation of water leaves empty space which, because of the topotactic relationship, occurs in certain energetically favored directions. Cavities are treated as empty nano-polyhedra, that is, a second phase which nucleates after dehydration for phase reconstruction and topotaxy favors it. In our case, both $Na_x(W,V)O_3.zH_2O$ and $(NH_4)_{0.33-x}(W,V)O_{3-y}$ present structures which are closely related to h-WO_3. When heating, water molecules leave their tunnel positions and sodium atoms are redistributed, modifying their position and causing the decrease in the volume of the unit cell according to previous reports.[4c, 32] In the same sense, NH_4^+ ions are eliminated from the hexagonal tunnels. As a result, crystal shrinkage occurs and reconstructive phase transformation takes place through the formation of the highly topotactic final product (h-WO_3 or h-$(W,V)O_3$ phase) together with nuclei of a secondary phase, as cavities can be considered, self-assembled along certain preferential crystallographic directions which are common with those of the starting phase.

Confirmation that crystals of our samples correspond to nanovoid-structured materials comes from the characterization performed by means of HAADF STEM. Since this detector uses the electrons scattered at high angles (*i.e.*, Rutherford scattering) for image formation, there is no phase contribution, the obtained images are very sensitive to the

atomic number *Z* (*Z*-contrast imaging) [34] and, therefore, to the crystal thickness. Under these conditions, nanocavities are observed as dark areas in the images (see figure 3). EELS analysis from spectra across the dark regions provide semiquantitative information about depth of the cavities. The analysis performed does not reveal the presence of other elements than W, V and O in the crystals or in the cavities and there is no chemical segregation associated with the contrasts observed. Figure 5 shows the high magnification Z-contrast images of two different crystals, (a) a rod-like crystal of the (NH_4^+)**W/V-O** sample and (b) a plate-like crystal of the (Na)**W/V-O** sample. The position of the EELS line-scans is indicated by the drawn lines and the profiles across the lines show the decrease in thickness in the corresponding dark areas. The measured depth is always around 10-15 nm.

The evolution of surface nanostructure has been further established through N_2 adsorption-desorption isotherms measurement by testing the behavior of samples heated at different temperatures. The N_2 adsorption-desorption isotherms corresponding to the (NH_4)**W/V-O** sample calcined at 250º C (a), 400º C (b) and 600º C (c) are shown in figure S4. The curve type of isotherms on figures (b) and (c) indicate mesoporosity in the materials in contrast with that of (a). The specific surface areas calculated by the BET method are 8, 20 and 30 m^2/g, respectively. These values suggest that elimination of ammonium and water when heating generates a high surface area from internal interfaces, in agreement with the HAADF-STEM observations.

The hexagonal form of WO_3, h-WO_3, has always been referred in the literature as a metastable phase. [30,31] A recent investigation on the formation of h-WO_3 from hexagonal ammonium tungsten bronze provided evidence about the structural framework collapse when NH_4^+ is completely released from the structure.[4a] Authors propose that the structure of h-WO_3 cannot be maintained without traces of stabilizing

ions or molecules in the hexagonal channels. Based in their thermoanalytical and solid state studies, they found a parallelism between the complete elimination of NH_4^+ and the collapse of h-WO_3 and its transformation into m-WO_3. In our samples, both ammonium and/or alkali metals have played the role of structure directors during the synthesis process. After NH_4^+ evolution, the V-free material is transformed into m-WO_3. The evolved gas analytical curves displayed on figure S5 show the release of NH_3 beginning at ~ 200º C for the W-O sample and above 300º C for the W/V-O material. In addition, water is eliminated in two steps, the first one at about 250º C is common in both curves but the second one occurs at 400º C for the V-free sample and at 500º C for the V-containing sample. Water eliminated at these high temperatures is explained as combustion product of the as-released NH_4^+ and the higher temperature in V-containing sample can be related to the fact that ammonium is more tightly retained in this framework. In fact, the V-containing sample retains the h-WO_3 form up to 600º C (see figure S2). In the Na samples, heat-treatment leads to the release of water but sodium remains in the structure. However, the hexagonal phase is not retained in the V-free sample. Therefore, it seems that it is the addition of vanadium the factor that rises up the stability range of the hexagonal phase which became a stable polymorph at 600ºC and it is the high thermal stability of this phase what has made possible to study the evolution of surface microstructure with temperature.

At this point we should emphasize that cavities are not responsible for the streaking observed, as deduced from the careful processing of the image contrast in the micrographs areas.

Nanocavities play an important role in the enhancement of the functional properties of the solids. This is the case of the photoreactivity of TiO_2-anatase nanorods, [18] the electrochemical lithium insertion properties of TiO_2-B [33] or the excellent adsorption

performance of $WO_3.0.33H_2O$ obtained from partial dehydration of $WO_3.H_2O$.[15] In this sense, the potential relevance that nanocavities may have in the surface properties of these materials has been tested by using them as redox catalysts in the partial oxidation of H_2S to sulphur. This study has been carried out at moderate temperatures (i.e. lower than 250ºC) in order to ensure no modification on the surface features occurs as a result of the temperature of the catalytic process. Creating porosity in a solid catalyst may be a method to modify the density of active sites and/or to provide extra accessibility. Therefore, it allows establishing the influence of the surface microstructure on the catalytic performance by comparison of the results obtained on the materials heat-treated at different temperatures. Figure 6 shows the variation of the specific catalytic activity (in mmol $_{H2S}$ m^{-2}) with reaction temperature achieved during the partial oxidation of H_2S. Catalytic tests have been done on (NH_4)**W/V-O** pristine sample and the corresponding samples after treatments at 250, 400 or 600º C in N_2 atmosphere. In all cases, the selectivity to sulfur was higher than 98%. Although similar catalytic activity for both the pristine sample and the sample heat-treated at 250ºC is observed, it increases when increasing the calcination temperature. As previously mentioned, once the water and/or ammonium molecules depart from the crystals thus leaving empty spaces, the structure begins to rearrange progressively when rising temperature and the empty spaces became self-assembled nanocavities along certain crystallographic directions. The heat-treatment process does not change the nature of active centers of the catalysts which are mainly related to the V-atoms isomorphously incorporated in the structural framework.[7] These results suggest changes in the density of active sites when increasing the heat-treatment. Since there is preferential growth along the [001] direction most of the crystal area is oriented perpendicular to the (001) plane and access is restricted. Accordingly, the presence of cavities provides additional accessibility to

the active centers of the structure and the consequence is a final enhancement of the catalytic performance for the highest heat-treatment temperature.

In summary, the synthesis route followed to prepare *h*-$(W,V)O_3$ from $Na_x(W,V)O_3.zH_2O$ and $(NH_4)_{0.33-x}(W,V)O_{3-y}$ has led to a nanostructured material by means of the formation of a dense population of regular and self-organized nanocavities on the crystals surface. The topotactic relationship between the as-synthesized product and the desired heat-treated final product is proposed as the origin of the surface nanostructure, after elimination of water and/or ammonium species.

A broader treatment of the results achieved could spread the approach to different materials obtained by chemical reactions of solids leading to products with defined crystallographic orientation with respect to the original crystal by exchanging components with the surroundings. Mild synthesis conditions provided by the hydrothermal processes are probably necessary and different degrees of conservation of structural elements can occur as exemplified by TiO_2 obtained from $H_2Ti_3O_7$ [18] or by $WO_3.0.33H_2O$ obtained from $WO_3.H_2O$[16] that retain certain crystallographic relationships with their precursors or by $(W,V)O_3$ where there exists a close structural relationship by keeping the three-dimensional skeleton. The incorporation of this approach to materials displaying different abilities may improve their chemical/physical final properties.

ACKNOWLEDGMENT

Authors acknowledge the financial support from DGICYT in Spain through projects MAT2010-19837-C06-05 and CTQ2012-37925-C03-1. Authors are also grateful to the Centro de Microscopia Electrónica (UCM) for facilities.

REFERENCES

1. (a) M Shibuya and M., Miyauchi, *Chem. Phys. Lett.* 2009, **473**, 126; (b) S. Balaji, Y. Djaoued, A. S., Albert, R. Z., Ferguson and R. Bruning, *Chem. Mater.* 2009, **21**, 1381; (c) W. Han, M. Hibino and T. Kudo, *Solid State Ionics* 2000, **128**, 25.

2. (a) A. Ponzoni, E. Comini, S G. Berveglieri, J. Zhou, S. Z., Deng, N. S. Xu, Y. Ding, Z. L. Wang, *Appl. Phys. Lett.* 2006, **88**, 20310, (b) J. Polleux, A. Gurlo, N. Barsan, U. Weimar, M. Antonietti and M. Niederberger, *Angew. Chem., Int. Ed.* 2006, **45**, 261, (c) I. M. Szilagyi, L. S.Wang, P. I. Gouma, C. Balaszsi, J. Madarasz and G. Pokol, *Mater. Res. Bull.* 2009, **44**, 505, (d) S. Pokhrel, C. E. Simion, V. S. Teodorescu, N. Barsan and U. Weimar, *Ad*v. *Funct. Mater.* 2009, **19**, 1767, (e) G. Wang, Y. Ji, X. R. Huang, X. Q. Yang, P. I. Gouma and M. Dudley, *J. Phys. Chem. B* 2006, **110**, 23777, (f) X. L.Li, T. J. Lou, X. M. Sun and Y. D. Li, *Inorg. Chem.* 2004, **43**, 5442.

3. I. M. Szilágyi, B. Fórizs, O. Rosseler, Á. Szegedi, P. Németh, P. Király, G. Tárkányi, B. Vajna, K. Varga-Josepovits, K. László, A. L. Tóth, P. Baranyai and M. Leskelä, *J. Catal.* 2012, **294**, 119.

4. (a) I. M. Szilagyi, J. Madarasz, G. Pokol, P. Kiraly, G. Tarkanyi, S. Saukko, J. Mizsei, A. L. Toth, A. Szabo and K. Varga-Josepovitso, *Chem. Mater.* 2008, **20**, 4116, (b) C. S. Griffith, F. Sebesta, J. V. Hanna, P. Yee, E. Drabarek, M. E. Smith and V. Luca, *J. Nucl. Mater.* 2006, **358**, 151, (c) C. S. Griffith, V. Luca, J. V. Hanna, K. J. Pike, M. E. Smith and G. S. Thorogood, *Inorg. Chem.* 2009, **48**, 5648, (d) Z. Gu, H. Li, T. Zhai, W. Yang, Y. Xia, Y. Ma and J. Yao, *J. Solid State Chem.* 2007, **180**, 98.

5. Y. Zhou, K. Zheng, J.-D. Grunwaldt, T. Fox, L. Gu, X. Mo, G. Chen and G. R. Patzke, *J. Phys. Chem. C* 2011**, 115***,* 1134.

6. (a) M. Schiavello, F. Pepe, M. Cannizzaro, A. De Rossi and R. J. D. Tilley, Z. *Phys. Chem. Neue Folge* 1977, **106**, 45, (b) J. Haber, J. Janas, M. Schiavello and R. J. D. Tilley, *J. Catal*. 1983, **82**, 395.

7. M. D. Soriano, P. Concepción, J. M. López Nieto, F. Cavani, S. Guidetti and C. Trevisanut, *Green Chem.*, 2011, **13**, 2954.

8. (a) Ch. Yu, L. Zhang, J. Shi, J. Zhao, J. Gao and D. Yan, , *Adv. Funct. Mater.* 2008, **18**, 1544. (b) J. Zheng, Z.-Y. Jiang, Q. Kuang, Z.-X. Xie, R.-B. Huang and L.-S. Zhen, *J. Solid State Chem.* 2009, **182**, 115.

9. A. Michailovski, R. Kiebach, , W. Bensch, , J.-D. Grunwaldt, A. Baiker, S. Komarneni and G.R. Patzke, *Chem. Mater.* 2007, **19**, 185.

10. R. Kiebach, N. Pienack, W. Bensch, J.-D. Grunwaldt, A.Michailovski, A. Baiker, T. Fox, Y. Zhou and G. R. Patzke*; Chem. Mater.* 2008**, 20***,* 3022.

11. Y. Zhou, N. Pienack, W. Bensch and G. R. Patzke, *Small* 2009, **5(17)**, 1978.

12. J. Shi, G. Hu, R. Cong, H. Bu and N. Dai, *New J. Chem.*, 2013, **37**, 1538.

13. D. L. Chen, L. Gao, A. Yasumori, K. Kuroda and Y. Sugahara, *Small* 2008, **4**, 1813.

14. L. Zhou, J. Zou, M. M. Yu, P. Lu, J. Wei, Y. Q. Qian, Y. H. Wang and C. Z. Yu, *Cryst. Growth Des.* 2008, **8**, 3993.

15. J. Yang, L. Jiao, Q. Zhao, Q. Wang, H. Gao, Q. Huan, W. Zheng, Y. Wang and H. Yuan, *J. Mater. Chem.* 2012**, 22**, 3699.

16. B. Liu, J. Wang, J. Wu, H. Li, Z. Li, M. Zhou, T. Zuo, *J. Mater. Chem. A* 2014, **2**, 1947.

17. M. Banerjee, S. K. Datta and H. Saha, *Nanotechnology* 2005, **16**, 1542, D. Majumdar, S. Chatterjee, M. Dhar, S. K. Dutta and H. Saha, *Sol. Energy Mater. Sol. Cells* 2003, **77**, 51.

18. W.Q. Han, L. Wu, R.F. Klie and Y. Zhu, *Adv. Mater.* 2007, **19**, 2525**.**

19. D.R. Rolison, *Science* 2003**, 299**, 1698.

20. Egerton, R. F. *Electron Energy-Loss Spectroscopy in the Electron Microscope*; Plenum Press: New York, 1996.

21. M.D. Soriano, J. Jiménez-Jiménez, P. Concepción, A. Jiménez-López, E. Rodríguez-Castellón and J.M. López Nieto, *Appl. Catal. B: Environ.* 2009**, 92**, 271.

22. K. P. Reis, E. Prince and M. S. Whittingham, *Chem. Mater.* 1992, **4**, 307.

23. B. Gerand, G. Nowogrocki and M. Figlarz, *J. Solid State Chem.* 1981, **38**, 312.

24. J. Pannetier, *Chemica Scripta* 1986**, 26A**, 131.

25. L. Seguin, M. Figlarz and J. Pannetier, *Solid State Ionics* 1993, **63-65**, 437.

26. B. Gerand, G. Nowogrocki, J. Guenot and M. Figlarz, *J. Solid State Chem.* 1979, **29**, 429.

27. A. Magneli, *Acta Chem. Scand.* 1953, **7**, 315.

28. V. A. Isupov, *Ferroelectrics* 1998, **211**, 209.

29. (a) B. O. Loopstra and P. Boldrini, *Acta Crystallogr*. 1966, **B21**, 158, (b) B. O. Loopstra and H. M. Rietveld, *Acta Crystallogr*. 1969, **B25**, 1420.

30. M. Figlarz, *Prog. Solid St. Chem.* 1989, **19**, 1.

31. Ph. Labbe, *Key Eng. Mat.* 1992, **68**, 293.

32. V. Luca, C. S. Griffith and J. V. Hanna, *Inorg. Chem.* 2009, **48**, 5663.

33. Q. Li, J. Zhang, B. Liu, M. Li, R. Liu, X. Li, H. Ma, S. Yu, L. Wang, Y. Zou, Z. Li, B. Zou, T. Cui and G. Zou, *Inorg. Chem.* 2008**, 47**, 9870.

34. S. J. Pennycook, *Ultramicroscopy* 1989, **30**, 58.

TABLES

Table 1. Synthesis parameters for the preparation of V-free and V-containing HTB-type phase.

Sample	Oxalic acid/W molar ratio	V/W atomic ratio	NaCl/W molar ratio	$Na_2WO_4/(NH_4)_6H_2W_{12}O_{40}$ molar ratio
(Na)**W-O**	0.07	-	-	∞
(NH_4^+)**W-O**	0.07	-	-	0
(Na/ NH_4^+)**W-O**	0.07	-	0.05	0
(Na)**W/V-O**	-	0.2	-	∞
(NH_4^+)**W/V-O**	-	0.2	-	0
(Na/ NH_4^+)**W/V-O**	-	0.2	0.33	0

Table 2. Stability of the HTB-type phase in pristine and heat-treated samples.

	PRISTINE SAMPLES		***HEAT-TREATED SAMPLES***	
	Formation of HTB-type phase		***Stability of HTB-type phase***	
Template cation	**W-O**	**W/V-O**	**W-O**	**W/V-O**
Na^+	Formed	Formed	Unstable	Stable up to 600º C
NH_4^+	Formed	Formed	Stable up to 450º C	Stable up to 600º C
Na^+/NH_4^+	Formed	Formed	Stable up to 450º C	Stable up to 600º C

FIGURES

Figure 1. Selected area electron diffraction patterns (SAED) corresponding to three different crystals in the (a) [100], (b) $[1\bar{1}0]$ and (c) [001] zone axes.

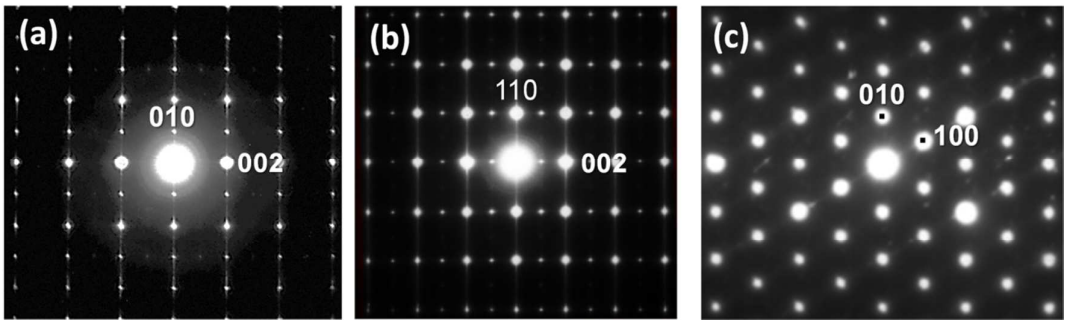

Figure 2. High resolution electron micrographs of three different crystals in the (a) [100], (b)) $[1\bar{1}0]$ and (c) [001] projections.

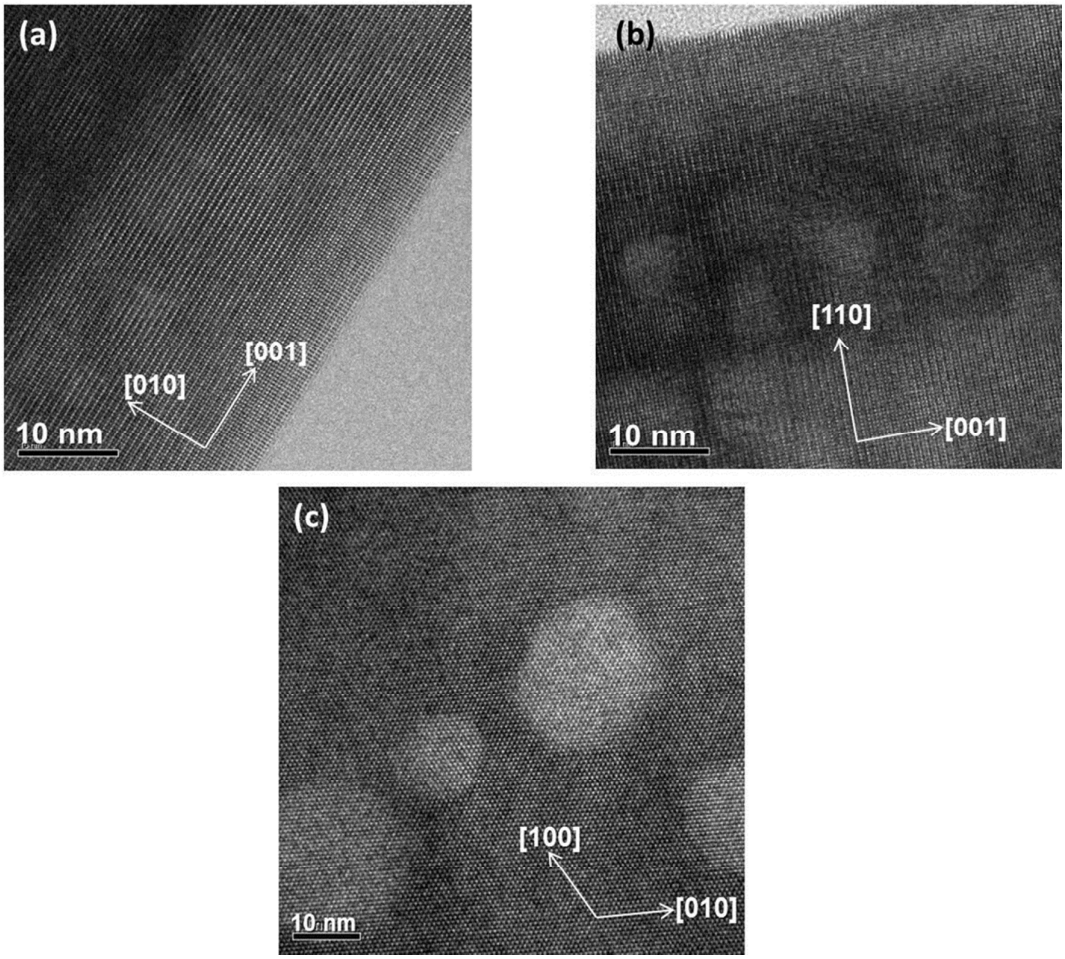

Figure 3. Low magnification HAADF-STEM micrographs showing the nanocavities on the surface of two different crystals calcined at 250º C (a) and 600º C (b).

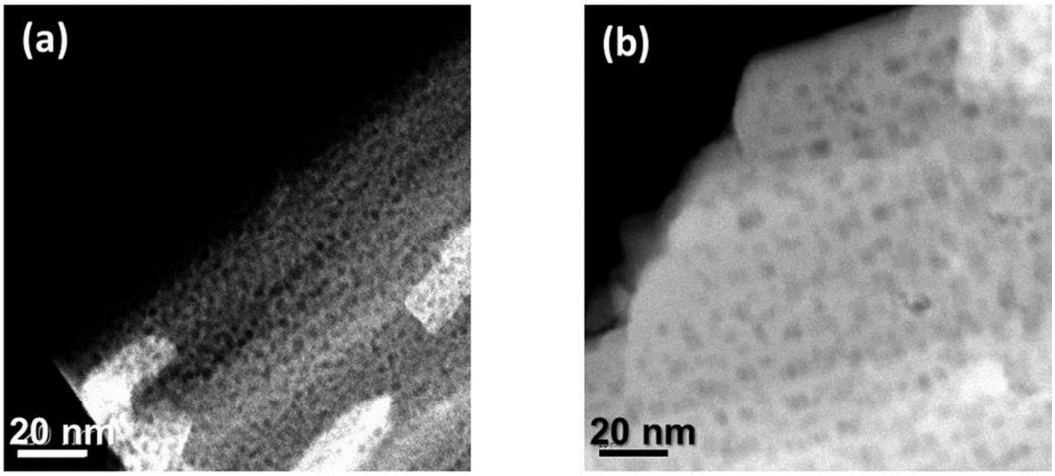

Figure 4. Simultaneous TG-DTA curves measured in air of the W-O and W/V-O series containing Na^+ (a), NH_4^+ (b) and Na^+ / NH_4^+ (c).

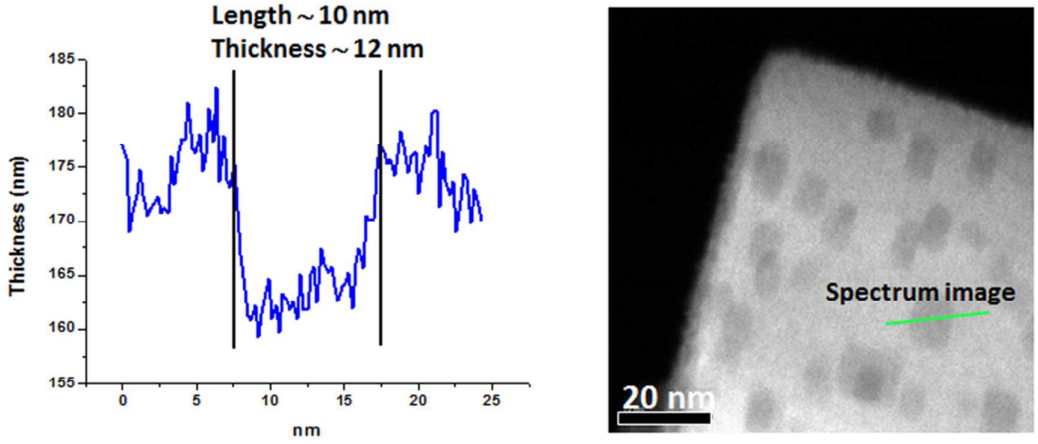

Figure 5. High magnification HAADF-STEM micrographs of two different crystals, (a) rod-like crystal of the (NH_4^+)**W/V-O** sample and (b) plate-like crystal of the (Na)**W/V-O** sample. The position of the EELS line scan is shown on each image together with the corresponding thickness profile.

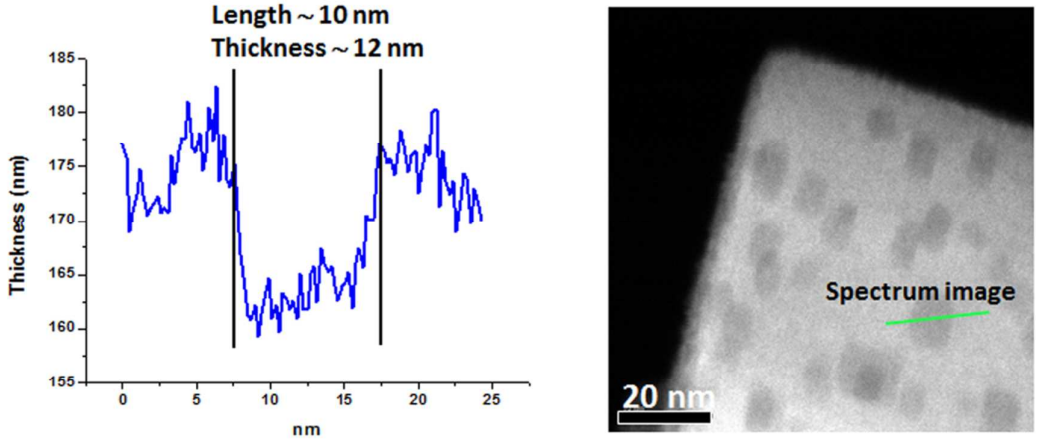

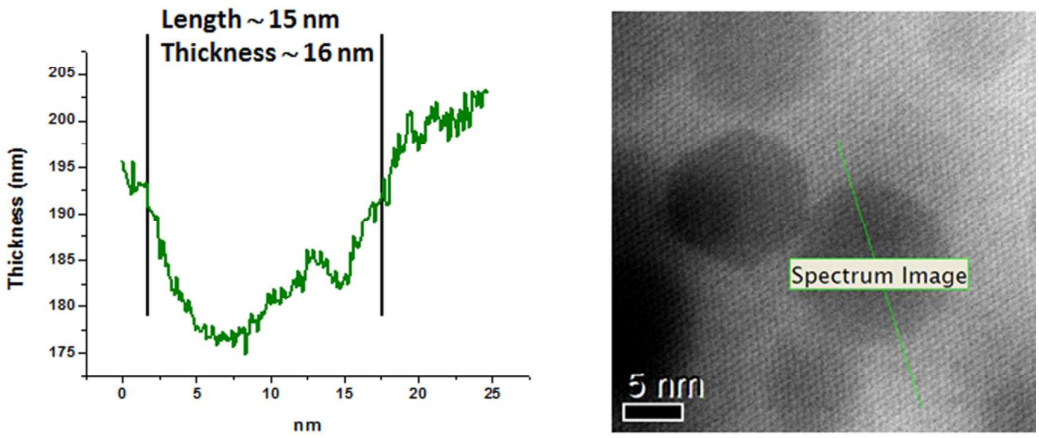

Figure 6. Specific catalytic activity for partial oxidation of H_2S to sulphur over (NH_4)**W/V-O** samples: as-synthesized (□) or heat-treated at 250 (○), 400 (Δ) or 600 ºC (◊).